REPORT DOCUMENTATION PAGE

Form Approved
OMB No. 0704-0188

PLEASE DO NOT RETURN YOUR FORM TO THE ABOVE ADDRESS.

1. REPORT DATE *(DD-MM-YYYY)*	2. REPORT TYPE	3. DATES COVERED *(From - To)*
20-04-2009	REPRINT	

4. TITLE AND SUBTITLE

A preliminary comparison of daylit and night C_n^2 profiles measured by thermosonde

5a. CONTRACT NUMBER

5b. GRANT NUMBER

5c. PROGRAM ELEMENT NUMBER

62601F

6. AUTHOR(S)

John R. Roadcap and Paul Tracy

5d. PROJECT NUMBER

1010

5e. TASK NUMBER

OT

5f. WORK UNIT NUMBER

A1

7. PERFORMING ORGANIZATION NAME(S) AND ADDRESS(ES)

Air Force Research Laboratory/RVBY
29 Randolph Road
Hanscom AFB MA 01731-3010

8. PERFORMING ORGANIZATION REPORT NUMBER

AFRL-RV-HA-TR-2009-1032

9. SPONSORING/MONITORING AGENCY NAME(S) AND ADDRESS(ES)

10. SPONSOR/MONITOR'S ACRONYM(S)

11. SPONSOR/MONITOR'S REPORT

12. DISTRIBUTION/AVAILABILITY STATEMENT

Approved for Public Release; Distribution Unlimited

13. SUPPLEMENTARY NOTES

REPRINTED FROM: RADIO SCIENCE, Vol 44, RS2001, doi: 10.1029/2008RS003921, 2009

14. ABSTRACT

The refractive index structure constant C_n^2 is needed to characterize optical wave propagation in a refractive turbulent scattering medium. A limited number of in situ measurements of C_n^2 made during day and night conditions from the surface to 10 km above sea level are compared in three different atmospheric boundary layer environments: dry convective, moist convective, and marine inversion. C_n^2 on average appears to be higher through the convective boundary layer depth during the day compared to night for the same air mass type and location but is generally lower than night values within the stable marine inversion layer. Calculations of path scintillation effects for slant paths in the lower atmosphere at near-infrared wavelengths are also compared for day and night conditions associated with the different air mass types.

15. SUBJECT TERMS

Optical turbulence Thermosonde C_n^2 Boundary layer

16. SECURITY CLASSIFICATION OF:			17. LIMITATION OF ABSTRACT	18. NUMBER OF PAGES	19a. NAME OF RESPONSIBLE PERSON
a. REPORT	b. ABSTRACT	c. THIS PAGE			John Roadcap
UNCLAS	UNCLAS	UNCLAS	SAR		19b. TELEPHONE NUMBER *(Include area code)*

Standard Form 298 (Rev. 8/98)
Prescribed by ANSI Std. Z39.18

RADIO SCIENCE, VOL. 44, RS2011, doi:10.1029/2008RS003921, 2009

A preliminary comparison of daylit and night C_n^2 profiles measured by thermosonde

John R. Roadcap[1] and Paul Tracy[1]

Received 31 May 2008; revised 15 December 2008; accepted 26 January 2009; published 28 March 2009.

[1] The refractive index structure constant C_n^2 is needed to characterize optical wave propagation in a refractive turbulent scattering medium. A limited number of in situ measurements of C_n^2 made during day and night conditions from the surface to 10 km above sea level are compared in three different atmospheric boundary layer environments: dry convective, moist convective, and marine inversion. C_n^2 on average appears to be higher through the convective boundary layer depth during the day compared to night for the same air mass type and location but is generally lower than night values within the stable marine inversion layer. Calculations of path scintillation effects for slant paths in the lower atmosphere at near-infrared wavelengths are also compared for day and night conditions associated with the different air mass types.

Citation: Roadcap, J. R., and P. Tracy (2009), A preliminary comparison of daylit and night C_n^2 profiles measured by thermosonde, *Radio Sci.*, *44*, RS2011, doi:10.1029/2008RS003921.

1. Introduction

[2] The U.S. Air Force Research Laboratory (AFRL) recently demonstrated a capability to make in situ measurement of index of refraction structure constant C_n^2 profiles during both daytime (daylit or sun above horizon) and at night (sun below horizon at measurement altitude) using balloon-borne thermosondes. Until recently, thermosonde measurements had been conducted principally at night, i.e., in darkness, to avoid solar-related effects on the thermal probes. A comparison of the two measurement conditions, day and night, is described using these measurements which occurred in three different atmospheric boundary layer environments. Even though the profiles are relatively few in number, these measurements should be of interest to those modeling optical properties of the troposphere.

2. C_n^2 and Thermosonde Measurements

2.1. Refractive Index Structure Constant C_n^2

[3] The magnitude of the index of refraction n turbulence spatial spectrum Φ_n or its structure constant C_n^2 is needed to characterize optical propagation in a turbulent forward scattering medium [e.g., *Martin and Flatte*, 1988]. The three-dimensional refractive index turbulence spectrum Φ_n for the inertial-convective range [see *Hill*, 1978] using the Kolmogorov power law model can be expressed as:

$$\Phi_n = 0.033 C_n^2 K^{-11/3} \qquad (\mathrm{m}^3) \qquad (1)$$

where $K = 2\pi/L$ is the spatial wave number and L is a spatial wavelength (m) characteristic of the refractive medium [*Churnside*, 1990] Typical scales of the inertial convective range for temperature fluctuations in the atmospheric boundary layer range from about 1 cm [*Hill*, 1978] to around several meters [*Dewan and Grossbard*, 2007]. At optical wavelengths, with the effects of humidity fluctuations neglected as specified in the original thermosonde instrument design, the refractive index structure constant is expressed in terms of the local background mean pressure p (hPa), mean temperature T (deg °K), and the temperature structure constant C_T^2 (°K^2 m$^{-2/3}$)

$$C_n^2 = \left(79 \times 10^{-6} \frac{p}{T^2}\right)^2 C_T^2 \quad \left(\mathrm{m}^{-2/3}\right) \qquad (2)$$

[*Clifford*, 1978].

[4] The humidity fluctuations' contribution to the index of refraction structure constant at optical wavelengths comes principally through the temperature-humidity covariance and can be ignored except in the marine surface layer or in the land surface layer over saturated soil [*Beland*, 1993]. For conditions of cold air blowing over a warm water surface, the surface layer

[1]Air Force Research Laboratory, Hanscom AFB, Massachusetts, USA.

contribution to refractive index variance has been measured as 81% temperature variance, 17% temperature-humidity covariance, and 2% humidity covariance [*Friehe et al.*, 1975]. For conditions where hot air blows over a saturated surface, the contribution of temperature-humidity covariance can equal or exceed that of temperature variance. All thermosonde launches described here occurred over a dry or unsaturated land surface.

[5] For a passive turbulent scalar such as temperature, assuming homogeneous, isotropic, and stationary behavior at inertial-convective-scale wavelengths and Kolmogorov's 2/3 power law, the temperature structure constant for a horizontal probe separation r, which lies within the inertial subrange, is:

$$C_T^2 = D_T r^{-2/3} \qquad \left(^\circ\mathrm{K}^2\ \mathrm{m}^{-2/3}\right) \tag{3}$$

where D_T is the temperature structure function:

$$D_T(\vec{r}) = \left\langle [T(\vec{r}_1) - T(\vec{r}_1 + \vec{r})]^2 \right\rangle \quad (^\circ\mathrm{K}^2) \tag{4}$$

[6] The angled brackets $\langle\ \rangle$ in (4) denote an ensemble time average. The temperature structure function can be described as the varying temporal mean of the square of a random temporally fluctuating temperature differential over a spatial separation r [*Beland*, 1993].

2.2. Thermosonde Measurements

[7] The thermosonde measures the temperature structure function D_T or structure constant C_T^2 over a one meter horizontal separation between two unheated tungsten fine wire probes to a resolution or noise floor limit of 0.002 °K and transmits these measurements at approximately one second intervals [*Jumper et al.*, 1999; *Kelley et al.*, 2005]. This places a noise floor limit of $\sim 4 \times 10^{-6}$ $\mathrm{K}^2\ \mathrm{m}^{-2/3}$ on the C_T^2 which can be measured by the thermosonde. When the thermosonde is attached to a balloon with a typical ascent rate of 5 m s^{-1}, this equates to C_T^2 root-mean-square (RMS) averaged measurements approximately every 5 m in the vertical. Thermosonde probe resistances and voltage noise floors are provided for each payload's electronics board for the C_T^2 calibration and calculation for each flight. An RMS chip is used to effect equation (4) for a 3.75 s time constant at probe sampling frequencies up to 200 Hz [*Jumper et al.*, 1999]. In addition to the temperature structure constant, the thermosonde measures the mean pressure, temperature, relative humidity, and wind speed and direction using an attached radiosonde. Thus, the refractive structure constant C_n^2 can be evaluated using equation (2).

[8] There are two principal components to the measurement uncertainty for altitudes below 10 km. One is caused by the noise level of the probes, mentioned above, and the other is the inherent uncertainty in estimating an ensemble average by the approximately 3.8 s average of the RMS chip. Both are reduced by averaging over a number of profiles. Numerical simulations of the RMS chip averaging by *Jumper et al.* [1999] using typical distributions of simulated turbulence showed random error factors of 10–20%. *Jumper et al.* [1999] also observed a dual time constant behavior which may contribute to a 20–30% increase in the turbulence. Representative error bars of 20% have been included on day C_n^2 profiles in Figures 1, 2, and 3 for comparison with measured layer values, along with a vertical profile of the approximate noise floor.

[9] Thermosonde measurements of C_n^2 can be made from the surface to 30 km above sea level. [see *Zink et al.*, 2004; *Roadcap and Murphy*, 1999]. During flight, thermosonde payloads must be suspended approximately 100 m below the balloon to avoid turbulent wake interference [*Kelley et al.*, 2005]. Beginning in 2006, advances in thermosonde probe board electronics which eliminated the noise floor drift due to solar heating effects below 25 km by decreasing the board current levels and in balloon launch reel technology which permits payload launches under high surface wind conditions, e.g., those associated with strong convective mixing, have allowed thermosonde launches and thus C_n^2 vertical profile measurements to occur in both daylit and night conditions. A comparison of the day and night measurements in the troposphere at altitudes less than 15 km for several campaigns is described below.

3. Comparison of Mean C_n^2 Profiles (Day and Night)

[10] Mean profiles of C_n^2 for five thermosonde measurement campaigns are used to compare the day and night launches. The campaign periods, locations and elevations, mean day boundary layer (BL) depths, and day versus night launch summary information are listed in Table 1. Boundary layer depth for each profile was determined using the thermosonde-measured vertical profiles of temperature and relative humidity and the vertical profile criteria for the type of boundary layer, such as those described in chapter 6 of *Garratt* [1994]. For the daylit convective boundary layer, extending above the convectively unstable surface layer, the boundary layer top was set equal to the top of the convectively mixed or dry adiabatic layer. The top of the marine inversion layer was usually associated with the top of a temperature inversion layer where the relative humidity or dew point began to sharply decrease with altitude. The nighttime boundary layer top, excluding the marine inversion cases, was associated with the top of an

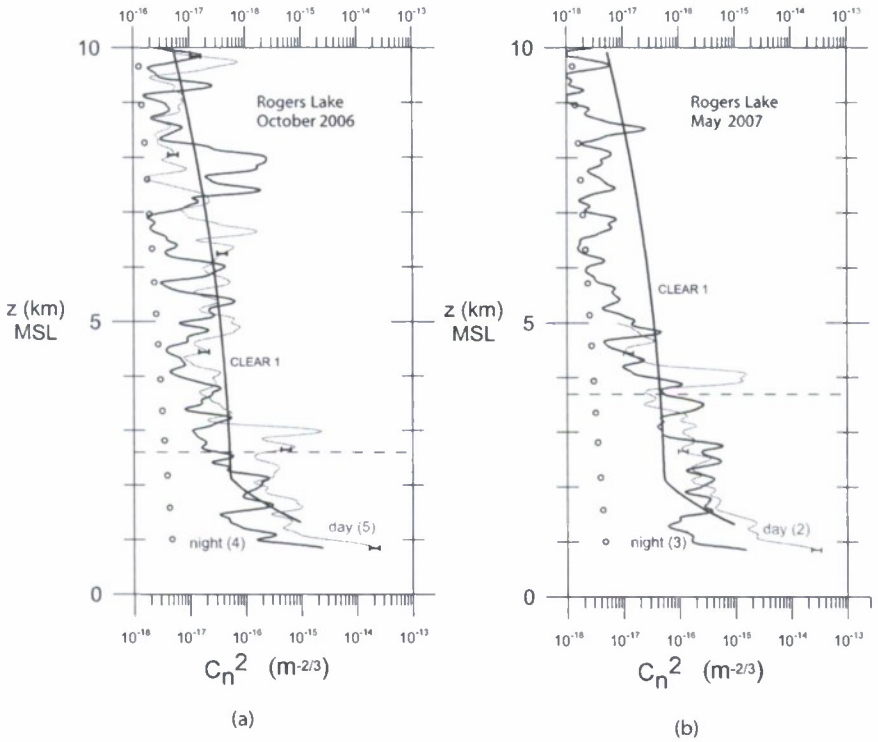

Figure 1. Dry convective. (a) Rogers Lake, California campaign, October 2006. (b) Rogers Lake, California campaign, May 2007. Circles mark noise floor. Error bars indicate instrumental uncertainty.

isothermal layer with enhanced relative humidity in approximately 3/4 of the cases.

3.1. Rogers Lake, California (Dry Convective)

[11] The measurement period of October 2006 for Rogers Lake, California (a desert area near Edwards Air Force Base (AFB)) was characterized by generally clear skies, strong daytime surface winds, and synoptic weather features associated with an active jet stream pattern over the western U.S. The boundary layer height ranged from 1.3 km to 3.7 km mean sea level (msl) and the tropopause height ranged from 10.6 km to 13 km. The mean daytime boundary layer height was 2.6 km above sea level.

[12] Figure 1a depicts the mean C_n^2 profile for day (red) and at night (blue) from the surface to 10 km above sea level (msl) for October 2006 on the basis of the available profiles. The numbers in parentheses show the number of profiles used to compute the mean. Each tick increment on the vertical axis represents 1 km. The black vertical profile is a nominal reference C_n^2 profile called CLEAR 1 [*Beland*, 1993]. The dashed horizontal line marks the mean daytime dry convective boundary layer top. Up to 3 km, the average daytime C_n^2 exceeds the nighttime value. Above 3 km, the dominance of either day or night in magnitude cannot be determined. A maximum in day time C_n^2 is evident just above the mean boundary layer top. Generation of optical turbulence by vertical shear and lapse rates associated with synoptic features such as jet streams, baroclinic zones, or atmospheric gravity waves may be the dominant source of turbulence in the levels above 4 or 5 km msl.

[13] Figure 1b is the same as Figure 1a but instead these data were taken for Rogers Lake Test area in May 2007. Like the October period, generally clear skies occurred during the measurement period with strong afternoon surface winds. Only two daytime and three nighttime measurement profiles were available. The average daytime C_n^2 profile exceeded the night measurements up to about 2 km msl. Another peak in daylit C_n^2 was observed just above the mean day BL top near 4 km. The mean day C_n^2 profile is capped at 5 km because of the occurrence of excessive noise above that altitude on one of the two day thermosonde launches.

3.2. Vandenberg AFB, California (Marine Inversion)

[14] Figure 2 compares the mean day and night profiles from thermosonde measurements made in the coastal

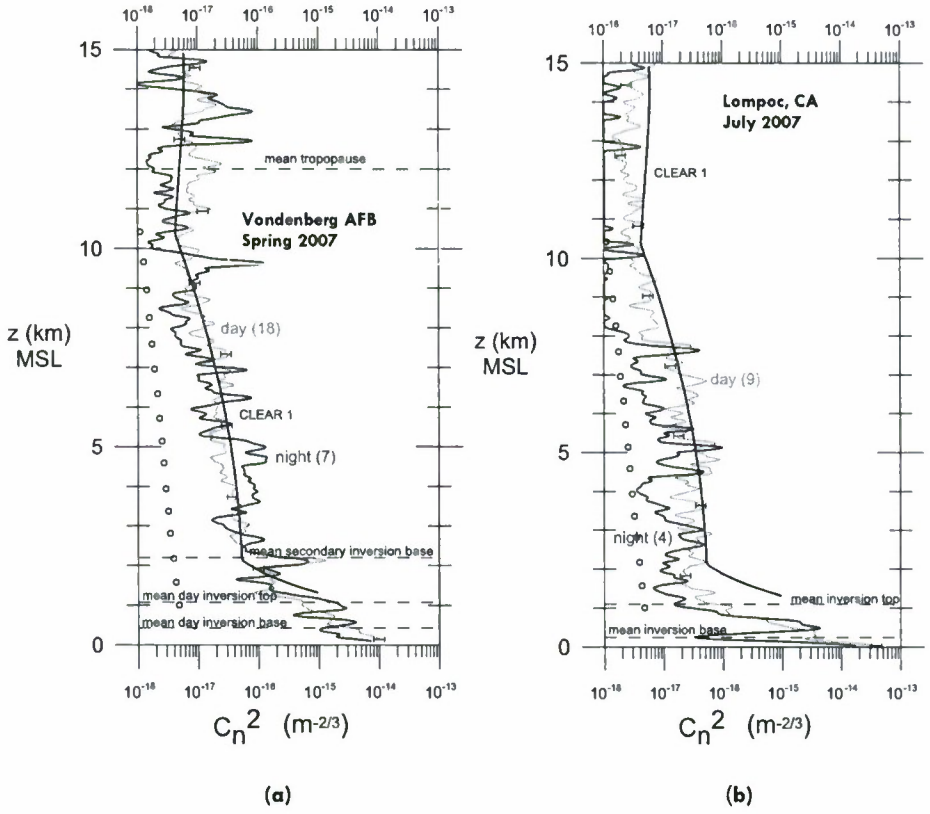

Figure 2. Marine inversion. (a) Vandenberg Air Force Base campaign, Spring 2007. (b) Lompoc, California campaign, July 2007. Circles mark noise floor. Error bars indicate instrumental uncertainty.

Pacific marine environment near Vandenberg AFB, California. Figure 2a depicts mean profiles taken during the Spring season (April–June) characterized by strong jet stream conditions in the upper troposphere and a marine inversion lower tropospheric environment. The marine inversion was sometimes accompanied by broken or overcast stratus clouds. The cloud layer typically began at the base of the inversion and ended at the inversion top. On average the marine inversion base occurred near 400 m with the inversion top around 1100 m. Marine stratus occurred during less than half of the daytime launches. In the marine inversion environment, on average the day C_n^2 exceeds the night values below the inversion base but was generally lower than the night values within the inversion layer. A secondary maximum of C_n^2 is found both day and night near the secondary inversion base located near 2.3 km. On the basis of the associated temperature and humidity profiles and daily synoptic weather maps, this secondary inversion base is associated with the eastern Pacific surface anticyclone. The mean tropopause height for this period averaged around 12 km.

[15] Figure 2b shows the mean C_n^2 profiles from thermosonde measurements taken at Lompoc, California (near Vandenberg) during late July 2007. The mean C_n^2 values were lower above 1 km compared to the Vandenberg measurements during the Spring period. Like the Spring Vandenberg means, C_n^2 was higher during the day below the inversion base and lower within the inversion compared to the night values. Above the inversion layer, mean day C_n^2 values were generally higher than the mean night values in the vertical profile. Also, above the inversion, both day and night mean C_n^2 is lower during the late July period at Lompoc compared to the mean C_n^2 at Vandenberg during the Spring measurements. The reduced average values above the marine inversion during July at Lompoc may be related to both (1) the more quiescent synoptic atmospheric conditions, including the absence of jet streams and strong vertical wind shear [*Businger et al.*, 2002], and (2) thermosonde

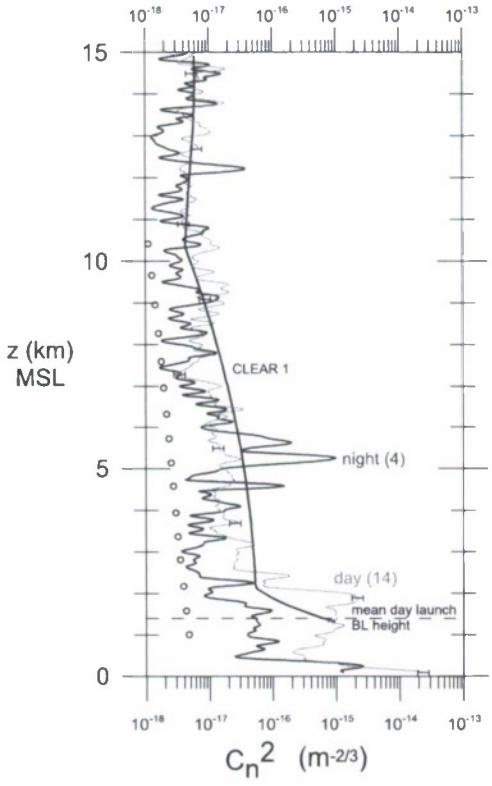

Figure 3. Moist convective at Fort Polk, Louisiana, July 2007. Mean tropopause height is near 15 m. Circles mark noise floor. Error bars indicate instrumental uncertainty.

trajectory paths, which tended to be over the water above 2 km, thus removing influences of complex terrain. The Spring Vandenberg sonde profile trajectories all were over land.

3.3. Fort Polk, Louisiana (Moist Convective)

[16] Figure 3 shows the mean profile of day and night C_n^2 for measurements made in a moist convective boundary layer environment at Fort Polk, Louisiana in July 2007, following the same labeling convention used in Figures 1 and 2. The mean daytime mixed layer depth was around 1.4 km with a mean tropopause height near 15 km. Sky conditions during day launches were characterized by clear or scattered low clouds although scattered or broken altocumulus and cirrus were often observed during the launches. Although the number of night measurements, compared to day measurements, is small, the day mean value exceeds the night mean from the surface to just above 3 km above sea level. A noticeable peak is evident above the top of the "mixed" layer around 2 km. This peak is similar in location relative to the mixed layer top which was observed in the dry convective environments of Rogers Lake. The peak in the mean night C_n^2 values just above 5 km is associated with the top of a persistent altocumulus layer.

4. Measurement of Surface C_n^2 Temporal Variation Compared With Ground Scintillometer

[17] The temporal variation of C_n^2 between daylit and night periods is displayed by a time sequence of thermosonde launches. Figure 4 depicts surface values of C_n^2 measured at thermosonde launch (circles) over a five day period and a time series of C_n^2 sampled once per minute by a ground scintillometer (black line) at Fort Polk.

[18] The scintillometer, whose horizontal propagation path was within 100 yards of the launch site, uses an optical measurement of scintillation index with a transmitter wavelength of 880 nm. The scintillometer instrument is a Scintec AG BLS900 Boundary Layer Scintillometer [*Scintec*, 2005] which consists of an optical transmitter, an optical receiver, and signal processing unit. The scintillometer measures log amplitude variance of the transmitted irradiance over a near-ground horizontal path and from that computes C_n^2. At Fort Polk, the scintillometer path length was approximately 800 m and the average path altitude was approximately 10 m above ground. The primary transmitter pulse repetition frequency

Table 1. Thermosonde Campaign Information

Location	Elevation (m msl)	Mean Day BL (km msl)	Period	Day/Night Profiles
Rogers Lake, California (35°N, 118°W)	846	2.6 (top)	Oct 2006	5/4
Vandenberg Air Force Base, California (35°N, 121°W)	99	0.4/1.1 (base/top)	Apr–June 2007	18/7
Rogers Lake, California	850	3.7 (top)	May 2007	2/3
Fort Polk, Louisiana (31°N, 93°W)	87	1.4 (top)	July 2007	14/4
Lompoc, California (35°N, 121°W)	29	0.3/1.1 (base/top)	July–Aug 2007	9/4
Total				48/22

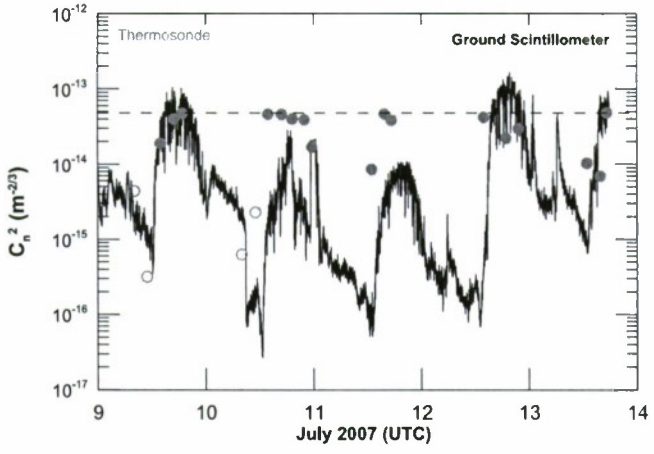

Figure 4. Time series of C_n^2 surface measurements at Fort Polk, July 2007. Each hash marks the date label in hours UTC.

was 25 Hz, with occasional measurements performed at 125 Hz, using an averaging period of one minute and data readout every minute.

[19] In Figure 4, the open circles represent surface values for night launches and the closed circles mark surface values for day launches. The upper dashed line represents the maximum value of C_n^2 allowed by the thermosonde board electronics. This can limit correlation with the highest surface values measured by the ground scintillometer. The "surface" value measured by the thermosonde occurs when the payload is held about one meter above ground immediately prior to balloon release. In practice, the thermosonde is continually repositioned to ensure the balloon's 100 m train will clear obstructions and to avoid ground contact following release. The C_n^2 minima observed by the surface time series typically occur around sunrise while the maxima usually occur during afternoon. Cloud cover or precipitation can modify this behavior. There is generally good correlation between the two instruments although the scintillometer measures lower peak values of surface C_n^2 during the day on 10 and 11 July.

5. Comparison of Path-Integrated Moments for Day and Night Measurements

[20] To quantify the differences between day and night C_n^2 profile magnitudes in terms of their effect on spatial resolution and amplitude scintillation, the coherence length r_0 (m) and Rytov variance σ_χ^2 were evaluated for three slant path configurations between the surface and 10 km above the surface. These are described further in section 5.2. For the evaluation, the spherical wave assumption is used with the direction of path integration being from ground-to-air or air-to-ground. The optical wavelength is set at 1.55 μm which corresponds to a commonly used near-infrared wavelength.

5.1. Computing Coherence Length and Rytov Variance for Slant Paths

[21] Fried's coherence length r_0 [*Fried*, 1966] determines the upper limit on the resolution imposed by the turbulent atmosphere which can be obtained from long exposure imaging. For the spherical wave approximation, this length is expressed as

$$r_0 = 2.1\left[1.46k^2 \int_0^S C_n^2(s)(s/S)^{5/3} ds\right]^{-3/5} \quad \text{(m)} \qquad (5)$$

[22] Here, $k = \frac{2\pi}{\lambda}$ is the optical wave number where λ is the optical wavelength. The integration is performed

Table 2. Fried's Coherence Length r_0 for Night/Day Launches (Low to High)[a]

Campaign	r_0 (sfc−10)	r_0 (sfc−4)	r_0 (4−10)	Number of Profiles
Rogers 2006	105/89	82/45	126/183	4/5
Rogers 2007	116/108	35/36	233/157	3/2
Vandenberg	76/91	29/35	148/162	7/18
Lompoc	147/99	63/54	256/166	4/9
Fort Polk	100/94	91/44	129/169	4/14
All	104/94	57/43	172/167	22/48

[a]Fried's coherence length given in cm for 30 km slant path integrated from lower to higher altitude. Parentheses enclose altitude range. Here sfc indicates surface.

Table 3. Fried's Coherence Length r_0 for Night/Day Launches (High to Low)[a]

Campaign	r_0 (sfc–10)	r_0 (sfc–4)	r_0 (4–10)	Number of Profiles
Rogers 2006	40/22	29/16	121/107	4/5
Rogers 2007	24/8	17/5	178/224	3/2
Vandenberg	11/8	7/5	65/93	7/18
Lompoc	12/8	7/5	121/77	4/9
Fort Polk	26/12	18/7	77/134	4/14
All	21/10	14/7	103/118	22/48

[a]Fried's coherence length given in cm for 30 km slant path integrated from higher to lower altitude. Parentheses enclose altitude range.

from the initial altitude ($s = 0$) to the desired altitude height Z at $s(Z)$ over the total slant path distance S. Tables 2 and 3 contain the path integrated results for r_0 performed for the lower-to-upper altitude and from the upper-to-lower altitude, respectively.

[23] For a point source with the direction of propagation extending from an initial altitude $s = 0$ to the altitude $s = S(Z)$, the Rytov approximation for the normalized intensity variance [see *Beland*, 1993] is expressed as

$$\sigma_\chi^2 = 0.56k^{7/6} \int_0^S C_n^2(s) \cdot [s(1 - s/S)]^{5/6} ds \qquad (6)$$

using the spherical wave assumption. The Rytov approximation ($\times 4$) is valid for scintillation index values up to $\sim$1.0 and does not account for the effects of saturation. Here, the Rytov approximation serves as a measure of the level of path-integrated optical turbulence and is independent of the direction of integration along the path. These results are presented in Table 4.

5.2. Slant Path Results

[24] The three slant path configurations each have a path length of 30 km. The first path, including both the boundary layer (BL) and "free" atmosphere above the BL, extends from the surface to 10 km above the surface. The second path, restricted to primarily the BL influence, extends in altitude from the surface to 4 km above the surface. The third configuration, free more or less from boundary layer influence, extends from 4 to 10 km above the surface. In Tables 2, 3, and 4, the number preceding the slash denotes a mean of the calculations using night measurement and the number following the slash denotes a mean of the calculations using daylit measurement. r_0 is listed in units of centimeters.

[25] The calculations indicate that slant paths residing at least in part in the boundary layer show significantly more path scintillation effects during day compared to night (Table 4, columns 2 and 3). The marine inversion regime (Vandenberg and Lompoc) exhibits, on average, smaller increase in scintillation effects during day compared to night for these paths. For viewing from overhead (Table 2), the atmosphere-limited resolution is generally better at night than during day for the boundary layer–influenced paths (columns 2 and 3). The exception is the Vandenberg measurement series which shows slightly higher atmosphere-limiting resolution during day compared to the night. For viewing from the ground (Table 3), the atmosphere-limited resolution is also better at night than during day, although mean coherence lengths are significantly smaller when viewing from the ground compared to viewing from overhead. This difference is due to the weighting of the C_n^2 profile toward the slant path end in equation (5), which is the surface for viewing from the ground and the upper altitude when viewing from overhead. For the free atmosphere paths, i.e., those primarily above the boundary layer (column 4), the scintillation effects (Table 4) are much smaller and the difference in scintillation on average between night and day appears small for all environments. Atmospheric resolution differences associated with the free atmosphere vary between campaigns (Tables 2 and 3, column 4). There is no clear indication that resolution is better during day or night. On average, the resolution is better for downward looking views (Table 2, column 4) compared to those viewing upward (Table 3, column 4). The higher overall scintillation levels at Vandenberg compared to Lompoc for boundary layer paths (Table 4, columns 2 and 3) are likely associated with over the land sonde trajectories which prevailed during the Spring Vandenberg measurements.

6. Summary and Conclusion

[26] A limited number of thermosonde launches have measured sequentially both daytime (sunlit) and nighttime (dark) vertical profiles of C_n^2. These measurements

Table 4. Rytov Variance σ_χ^2 for Night/Day Launches[a]

Campaign	σ_χ^2 (sfc–10)	σ_χ^2 (sfc–4)	σ_χ^2 (4–10)	Number of Profiles
Rogers 2006	0.03/0.11	0.06/0.37	0.03/0.02	4/5
Rogers 2007	0.05/0.15	0.18/0.46	0.004/0.04	3/2
Vandenberg	0.12/0.13	0.43/0.51	0.02/0.02	7/18
Lompoc	0.05/0.07	0.19/0.26	0.01/0.02	4/9
Fort Polk	0.05/0.14	0.06/0.56	0.04/0.01	4/14
All	0.07/0.12	0.22/0.46	0.02/0.02	22/48

[a]Rytov variance for 30 km slant path. Parentheses enclose altitude range.

have provided day and night C_n^2 relative to altitude range and air mass type. They have also demonstrated the possibility that the temporal and diurnal variation of the C_n^2 vertical profile below the tropopause can be captured by a sequence of thermosonde launches.

[27] Mean profiles suggest that C_n^2 is higher through the convective boundary layer depth and up to 0.5 km above the convective boundary layer top during the day compared to corresponding night measurements for the same air mass type and location. For the case of marine inversions, whose maximum depth ranges up to 1 km, on average the day C_n^2 exceeds the night values below the inversion base and in the surface layer but is often lower than the night values within the inversion layer.

[28] For path scintillation effects associated with a near-infrared point source at the ground, calculations indicate that slant paths residing in the boundary layer exhibit more scintillation during day compared to night with the convective boundary layer regime (Rogers Lake, Fort Polk) showing a larger night to day increase compared to the marine inversion cases (Vandenberg, Lompoc). For overhead viewing of points on the ground, the atmosphere-limiting resolution is generally better at night than during the day for boundary layer influenced paths. This day versus night behavior holds also for viewing from the ground although the mean coherence lengths in all campaigns are significantly lower compared to overhead views. For free atmosphere paths above the boundary layer, the difference in scintillation effects on average between nights and days appears negligible for all environments. Definitive conclusions await more measurements of the diurnal variation in C_n^2 vertical profiles.

[29] **Acknowledgments.** The day C_n^2 measurements were made possible in large measure by George Clement and Kris Robinson of Utah State University, who developed day and night thermosonde electronics configurations which could be launched in all weather conditions. MSgt Sandra Lewis and TSgt Paul Kammerman, USAF, made valuable contributions to the construction of the thermosonde electronic components and their deployment. The encouragement and advice of Bryce Schumm of AFRL's Sensors Directorate during the measurement campaigns is gratefully acknowledged. The authors also thank the anonymous reviewers whose comments significantly improved the paper.

References

Beland, R. R. (1993), Propagation through atmospheric optical turbulence, in *Atmospheric Propagation of Radiation*, vol. 2, pp. 157–232, Environ. Res. Inst. of Mich., Ann Arbor, Mich.

Businger, S., R. McLaren, R. Ogasawara, D. Simons, and R. J. Wainscoat (2002), Starcasting, *Bull. Am. Meteorol. Soc.*, *83*, 858–871, doi:10.1175/1520-0477(2002)083<0858:S>2.3.CO;2.

Churnside, J. H. (1990), A spectrum of refractive turbulence in the turbulent atmosphere, *J. Mod. Opt.*, *37*, 13–16, doi:10.1080/09500349014550031.

Clifford, S. F. (1978), The classical theory of wave propagation in a turbulent medium, in *Laser Beam Propagation in the Atmosphere*, pp. 9–43, Springer, Berlin.

Dewan, E. M., and N. Grossbard (2007), The inertial range "outer scale" and optical turbulence, *Environ. Fluid Mech.*, *7*, 383–396, doi:10.1007/s10652-007-9029-4.

Fried, D. L. (1966), Limiting resolution looking down through the atmosphere, *J. Opt. Soc. Am.*, *56*, 1380–1384, doi:10.1364/JOSA.56.001380.

Friehe, C. A., J. C. La Rue, F. H. Champagne, C. H. Gibson, and G. F. Dreyer (1975), Effects of temperature and humidity fluctuations on the optical refractive index in the marine boundary layer, *J. Opt. Soc. Am.*, *65*, 1502–1511, doi:10.1364/JOSA.65.001502.

Garratt, J. R. (1994), *The Atmospheric Boundary Layer*, 316 pp., Cambridge Univ. Press, Cambridge, U. K.

Hill, R. J. (1978), Models of the scalar spectrum for turbulent advection, *J. Fluid Mech.*, *88*, 541–562, doi:10.1017/S002211207800227X.

Jumper, G. Y., R. R. Beland, and P. Tracy (1999), Investigating sources of error in balloon-borne optical turbulence measurements, *Tech. Rep. AIAA 99–3618*, 9 pp., Am. Inst. of Aeronaut. and Astronaut., Reston, Va.

Kelley, M. C., C. Y. Chen, R. R. Beland, R. Woodman, J. L. Chau, and J. Werne (2005), Persistence of a Kelvin-Helmholtz instability complex in the upper troposphere, *J. Geophys. Res.*, *110*, D14106, doi:10.1029/2004JD005345.

Martin, J. M., and S. M. Flatte (1988), Intensity images and statistics from numerical simulation of wave propagation in 3-D random media, *Appl. Opt.*, *27*, 2111–2126.

Roadcap, J. R., and E. A. Murphy (1999), Comparison of isoplanatic angles derived from thermosonde and optical measurements, *Pure Appl. Geophys.*, *156*, 503–524, doi:10.1007/s000240050310.

Scintec AG (2005), Boundary layer scintillometer BLS450 BLS900 BLS200 user's manual, version 1.31, report, 57 pp., Tubingen, Germany.

Zink, F., R. A. Vincent, E. Murphy, and O. Cote (2004), Comparison of radar and in situ atmospheric measurements of turbulence, *J. Geophys. Res.*, *109*, D11108, doi:10.1029/2003JD003991.

J. R. Roadcap and P. Tracy, Air Force Research Laboratory, Hanscom AFB, MA 01731-3010, USA. (arfl.rvb.pa@hanscom.af.mil)